Materials Today: Proceedings xxx (xxxx) xxx

Contents lists available at ScienceDirect

Materials Today: Proceedings

journal homepage: www.elsevier.com/locate/matpr

Effect of printing parameters on microscale geometry for 3D printed lattice structures

Yagiz Kayali [a], Mingyang Ding [b], Sherif Hamdallah [c], Sheng Qi [c], Richard Bibb [d], Andrew Gleadall [a,*]

[a] Wolfson School of Mechanical, Electrical and Manufacturing Engineering, Loughborough University, Loughborough, UK
[b] Department of Mechanical Engineering, City University of Hong Kong, Hong Kong, China
[c] School of Pharmacy, University of East Anglia, Norwich, UK
[d] School of Design and Creative Arts, Loughborough University, Loughborough, UK

ARTICLE INFO

Article history:
Available online xxxx

Keywords:
Additive manufacturing
Printing parameters
X-ray micro-computed tomography
Optical microscopy
Surface quality

ABSTRACT

This study investigated the effect of manufacturing parameters on the manufacturing quality of material extrusion additive manufacturing (MEAM), specifically focusing on the microscale geometry of lattice structures built up by discrete extruded filaments. The manufacturing parameters extrusion height, printing speed and extrusion width were investigated. Square grid structures, which can be precisely characterized, were used to develop fundamental understanding that can be translated to more complicated structures in future investigations. Print paths were directly created as machine control code (GCode) using FullControl GCode Designer, bypassing the conventional multi-stage translation of a design from CAD to an STL file, to slicing software and finally to GCode. This allowed precise parametric control of all aspects of the manufacturing procedure, including aspects that would not be possible with conventional slicing software such as control over the specific order and direction of printing each line, and the offsetting of specific printed lines on each layer in the Z direction by half the layer height. The printing quality of the structures was investigated with optical microscope and X-ray micro-computed tomography (micro-CT). Microscale changes to the extruded-filament geometry were characterized before and after filament-crossing points in the square grid structure, and internal cavities were identified. Printing speed was found to be a crucial parameter that should be carefully considered for lattice structure applications that require high manufacturing quality in terms of minimizing microscale geometric defects. Offsetting crossing extrudates by half the layer-height in the Z direction resulted in more consistent microscale geometry and greatly improved quality.

1. Introduction

Material extrusion additive manufacturing (MEAM) has received significant attention for biomedical applications due to its great value [1]. There are many applications, including multi-material scaffolds [2,3], electronics components [4,5], customized skin, patient-specific implants [6,7] and sport related medical applications [8]. The popularity of MEAM is due to its widespread availability, low cost, low power consumption and ease of use of use.

MEAM is also promising for wound dressing applications. In contrast to commercialized wound dressings, additive manufacturing can help develop personalized wound dressings according to individual patients' requirements. Moreover, MEAM allows drug-loaded filaments to be used in 3D printing wound dressings [9,10].

Manufacturing quality, such as surface quality, is vital for biomedical applications including wound dressing applications. Therefore, understanding the effect of manufacturing parameters on geometry is vital to reaching optimum printing quality for biomedical applications. This research investigated extrusion width and height, printing speed, and cell size parameters to understand their effect on printing quality. A square grid structure was selected as the geometry to evaluate only the effects of manufacturing parameters. Instead of the conventional workflow of designing a 3D structure in computer-aided design software

* Corresponding author.
E-mail address: a.gleadall@lboro.ac.uk (A. Gleadall).

https://doi.org/10.1016/j.matpr.2022.08.487
2214-7853/

Please cite this article as: Y. Kayali, M. Ding, S. Hamdallah et al., Effect of printing parameters on microscale geometry for 3D printed lattice structures, Materials Today: Proceedings, https://doi.org/10.1016/j.matpr.2022.08.487

(CAD), before translating through several steps and different software to achieve a manufacturing procedure (GCode file), FullControl GCode Designer [11] was used to directly create the print path and intricately control all aspects of the manufacturing procedure. The effect of manufacturing parameters was evaluated with two imaging techniques: optical microscopy and X-ray micro-CT. Optical microscopy was used to assess surface related parameters, including the structure's geometry. X-ray micro-CT was used to evaluate features throughout the thickness of the extrudate and identify internal features such as cavities or cracks. This study develops new understanding about how the print path design and print parameters affect the microscale geometry of lattice structures and is currently being used to develop more complex lattices for wound dressing applications.

2. Methodology

This study had three main research stages: designing lattice structures with FullControl, 3D printing specimens, and optical analysis of specimens with microscope and/or X-ray micro-CT. An overview of the methodology is given in Fig. 1.

In the first part, GCode was created using FullControl GCode Designer [11]. FullControl is open-source software that allows users to control all aspects of the printing-path to print planar and non-planar geometries. Moreover, the software allows the user to directly control both geometric and non-geometric printing parameters. Additionally, since FullControl directly generates the gcode of design, there is no need to use any CAD or slicing software, allowing for a more streamlined parametric workflow and eliminating the risks of incremental errors (approximations) that are generated by conversion from CAD to STL and then slicing the STL file. [11]. The flowchart of FullControl software is given in Fig. 2.

In this study, the effect of manufacturing parameters on the geometry were evaluated by producing lattice structures. The specifications of the lattice structure are given in Fig. 3.

Parametric code was prepared with FullControl GCode Designer to manufacture the lattice structure shown in Fig. 3. Details of the design and parameters that were created for it are given in Fig. 4. In Fig. 4a, "layers" is the number of layers, "size" is the size of the square grid shown as "*L*" in Fig. 3, "x_start" and "y_start" are starting coordinate points of grid on the print platform, "EW" is the extrusion width of each extruded filament, "EH" is extrusion height of each extruded filament, and "cell_size" is the size of grid cells shown as "*l*" in Fig. 3. The feature-based design is shown in Fig. 4b. All designs used in this study are provided as supplementary material or can be obtained from the corresponding author.

After designing the lattice structure with FullControl, grid structures were manufactured with an Ultimaker 2^+ 3D printer using 3DXTECH branded polylactic acid (PLA) filament with a diameter of 1.75 mm. Nozzle diameter was selected as 0.4 mm which is commonly used in MEAM. Nozzle temperature and bed temperature were 210 °C and 60 °C, respectively as recommended by the material manufacturer. Material and printing properties are summarized in Table 1.

Parameters investigated in this study were printing extrusion width, extrusion height and printing speed. Several specimens were manufactured to examine the effect of these parameters. The matrix of variables for the printed specimens is given in Table 2.

Optical microscopy was used to investigate the top-surface of specimens, while micro-CT was implemented to evaluate the structures throughout the thickness direction and internally. A Zeiss Primotech optical microscope and a Nikon XTEK XT-H 160Xi micro-CT machine were used for this research. For X-ray micro-CT imaging, the effective pixel size was selected as 12.40 μm.

Images obtained from the X-ray micro-CT system were processed using CT PRO 3D software to build the 3D voxel volume model. Volume Graphics (VG) Studio Max software was utilized to analyse 3D voxel volume data.

3. Results and discussion

First, the effect of extrusion height was investigated. The extrusion width and printing speed were fixed at 0.50 mm and 1000 mm/min, respectively, to analyse the impact of extrusion height. Investigation of extrusion height was performed with X-ray micro–CT since surface characteristics did not change significantly according to optical microscopy investigation with changing extrusion height. However, the analysis showed some critical observations. Some cavities, for instance, were detected inside

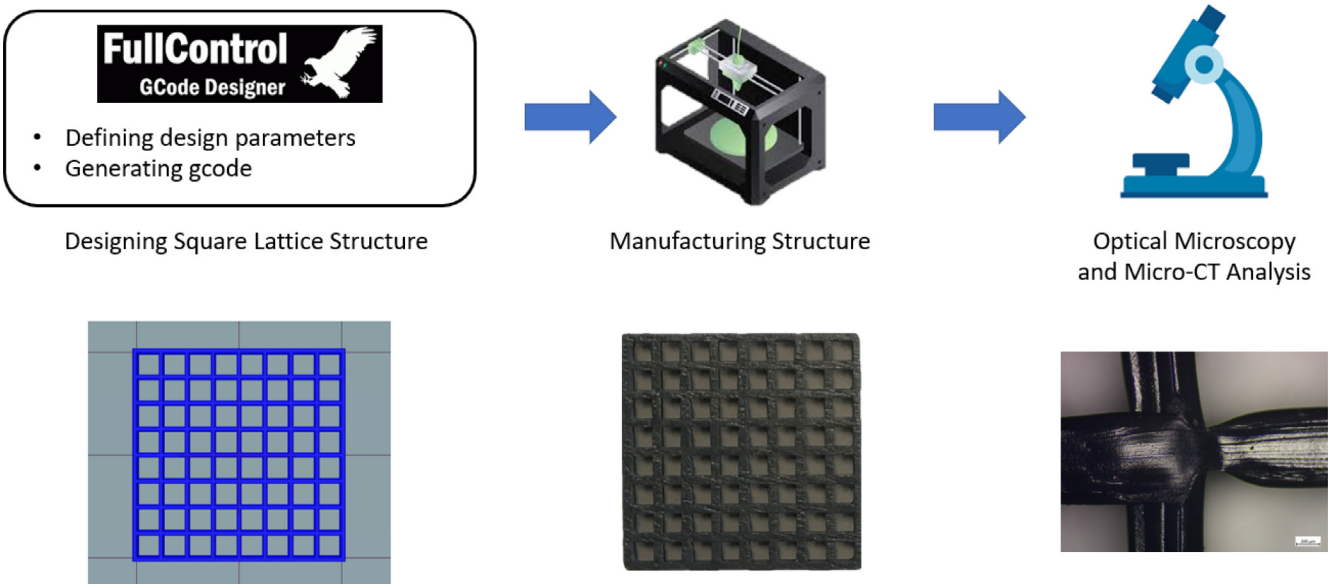

Fig. 1. Overview of Methodology.

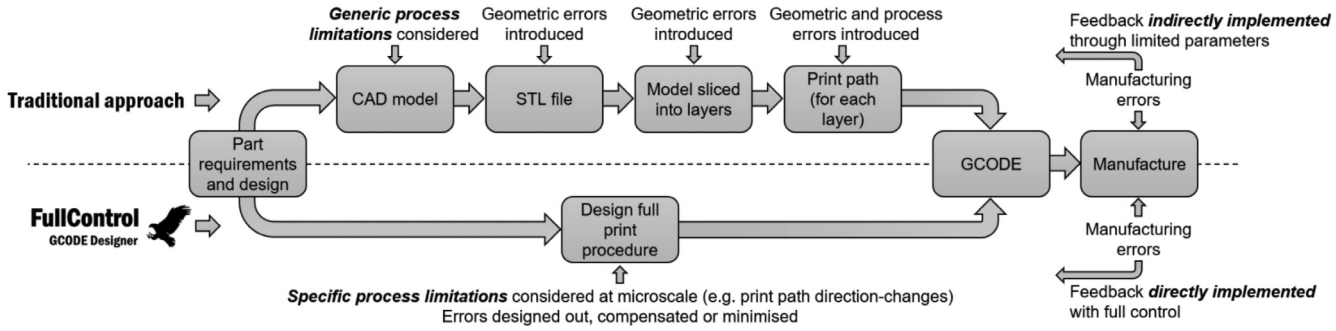

Fig. 2. Flowchart of FullControl GCode Designer (After [12]).

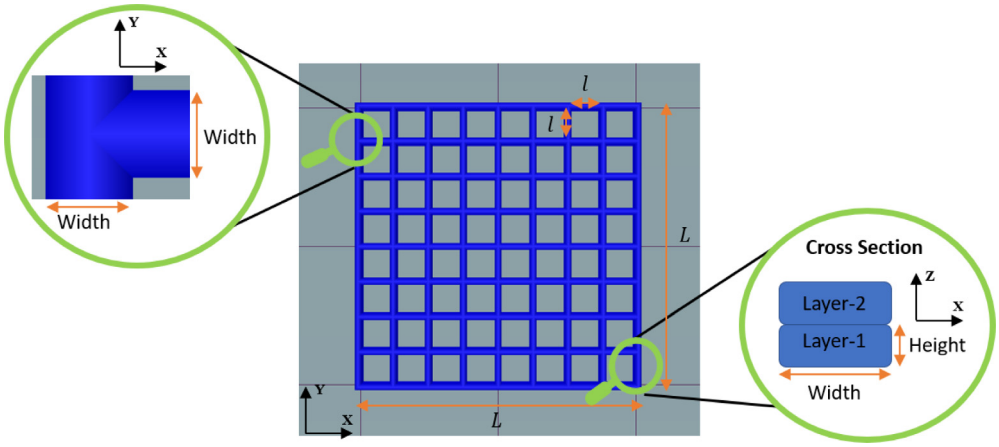

Fig. 3. General view of lattice structure.

the material. Some examples of the cavities detected are shown in Fig. 5.

In Fig. 5b, the high-density regions, (the PLA), are represented in green while low-density, (air), is shown in red colour. The observed trend indicates that these cavities generally occurred at the corners of cells. The main reason for the phenomenon might be the high viscosity of melted PLA. Due to the high viscosity of melted PLA, the material can become solidified before it reaches the left and right sides of previously extruded layers. Therefore, some cavities are generated at the right and left sides of the bottom layer of previously printed layers. This phenomenon is summarized in Fig. 6. Further micro-CT research is ongoing to develop greater understanding of internal cavities.

Apart from cavities, significant layer width variation was observed. Several factors can contribute to the variation of layer width, such as over extrusion or manufacturing tolerance of the printer. In particular, intersections of horizontal and vertical layers led to variation of extrusion width. This may have happened due to a build-up of pressure in the nozzle whilst printing vertical lines as it passed over previously printed horizontal lines (blocking extrusion). After the nozzle moved beyond the edge of horizontal lines, the built-up pressure may have been released through over-extrusion, resulting in wider vertical lines overall. This problem is likely to be more critical for shorter distances between parallel grid lines.

It can also be seen that extrusion width varied close to the cross-over point, with over-extrusion (wider filament) before crossing points and under-extrusion (narrower filament) after crossing points. This is to be expected and was seen in previous research due to a build-up of polymer (wider filament) as the nozzle pushes it into the edge of a previously printed line. In contrast, after crossing a previously printed line, there was a short delay before full extrusion width was achieved, leading to a small narrower region with a 'pinched' appearance.

The second group of specimens was manufactured to evaluate the effect of printing speed on surface quality. For this purpose, extrusion width and extrusion height were set as 0.5 and 0.2 mm, respectively, while printing speed changed as given in Table 2. Optical microscopy results of manufactured specimens with different printing speeds are shown in Fig. 7.

Results given in Fig. 7 show that printing speed has a significant influence on the final geometry of the specimens. Increasing printing speed resulted in unstable geometries. Vertical and horizontal lines deformed with increasing printing speed. Moreover, undesired geometries such as bulges started to occur, as seen in Fig. 7d–f.

Finally, the effect of extrusion width was evaluated by setting extrusion height and speed constant as shown in Table 2 from specimen ID 12 to15. The results are shown in Fig. 8.

Results given in Fig. 8 show significant width variation on both vertical and horizontal lines. The width of lines close to the intersection point of vertical and horizontal lines showed a considerable variation in extrusion width. A similar trend is also seen in Fig. 7. This might be due to over/under-extrusion. Similar geometric defects can be seen in all specimens even though extrusion width varied considerably from 75% to 175% of the nozzle diameter.

Over-extrusion, on the other hand, was separately investigated since it had a significant influence on microstructure. A grid structure was designed based on the details given in Fig. 3 to investigate the phenomena. For this grid structure, extrusion width, extrusion height and printing speed were selected as 0.5 mm, 0.2 mm and 1000 mm/s, respectively. In contrast to previous specimens in this

a

Parameter name	Parameter value	Units
layers	10	
size	20	
x_start	50	mm
y_start	50	mm
EW	0.5	mm
EH	0.1	mm
cell_size	2.5	mm

b

Feature												
1	Rectangle	50	50	70	R20	0	CW	0.5	0.1			
2	Line	Cartesian	R0	R0	R0	R0	R2.5	R0	Print	0.5	0.1	F=250
3	Line	Cartesian	R0	R0	R0	R20	R0	R0	Print	0.5	0.1	F=250
4	Line	Cartesian	R0	R0	R0	R0	R2.5	R0	Print	0.5	0.1	F=250
5	Line	Cartesian	R0	R0	R0	R-20	R0	R0	Print	0.5	0.1	F=250
6	Cartesian repeat	2-5	0	5	0	2						
7	Cartesian repeat	2-4	0	15	0	1						
8	Reflect	2-7	XY	50	50	70	70					
9	Postprocess	8	OffsetLinear	0	0	0	YES	YES				
10	Cartesian repeat	1-9	0	0	0.1	9						

c

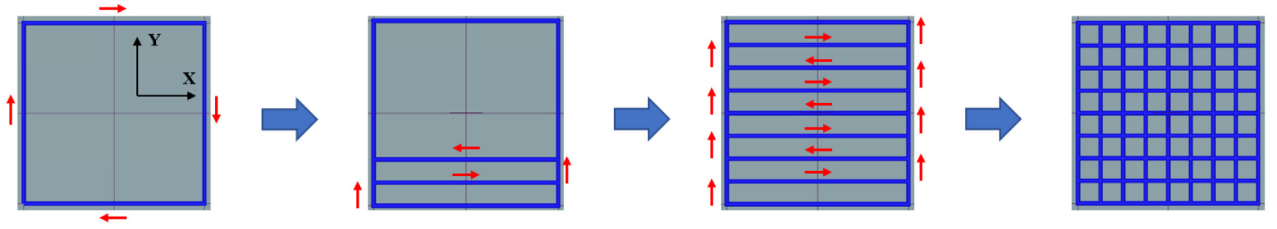

Feature 1
Generating rectangle

Feature 2 to 5
Printing the first two horizontal lines

Feature 6 to 7
Printing rest of the horizontal lines

Feature 8 to 10
Feature 8 and 9 reflect horizontal lines according to X and Y axis. Feature 10 repeats generated geometry 9 times

Fig. 4. Prepared GCode Designer code: (a) Parameters, (b) FullControl user-interface screen, and (c) Step-by-step analysis of FullControl Gcode Designer code.

Table 1
Summary of material and printing properties.

PLA Properties	Value	Printing Properties	Value
Density (g/cm^3)	1.24	Nozzle temperature (°C)	210
Glass transition temperature (°C)	55	Bed temperature (°C)	60
Melting temperature (°C)	160	Number of layers	10
		Nozzle diameter (mm)	0.4

Table 2
Printed specimens and their printing parameters.

Specimen ID	Extrusion Width (mm)	Extrusion Height (mm)	Printing Speed (mm/min)
1	0.50	0.10	1000
2	0.50	0.15	1000
3	0.50	0.20	1000
4	0.50	0.25	1000
5	0.50	0.30	1000
6	0.50	0.20	250
7	0.50	0.20	500
8	0.50	0.20	1000
9	0.50	0.20	2000
10	0.50	0.20	3000
11	0.50	0.20	4000
12	0.30	0.20	1000
13	0.40	0.20	1000
14	0.50	0.20	1000
15	0.70	0.20	1000

study, a 0.1 mm distance (in Z direction) was given between the vertical and horizontal paths. This is equivalent to offsetting half of the printed lines by half a layer in the Z direction. The effect of over- and under-extrusion at cross-over points was evaluated via optical microscope. The results obtained are given in Fig. 9. Extrusion width variation closer to cross-over of vertical and horizontal lines became less than in specimens without the previous geometries shown in Figs. 7 and 8. These results agree with simulation results using the VOLCO model [13], which predicted greater over-extrusion at crossover points when lines were printed closer together in the Z direction. Additionally, variation in extrusion width between horizontal and vertical lines was clearly reduced. Preliminary tensile-testing results from an ongoing study found that specimens with half-layer offsets in Z demonstrated over two-fold strength increases compared to specimens without the half-layer offset.

4. Conclusion

This research investigated the effect of printing parameters: extrusion height, extrusion width, and printing speed on the microscale geometry of MEAM grid structures. According to the results, the following conclusions are reported:

- X-ray micro-CT results showed that printed specimens had some internal cavities. These cavities were generally observed around the corners of cells. Therefore, these regions are vulnerable sections for forming cavities.

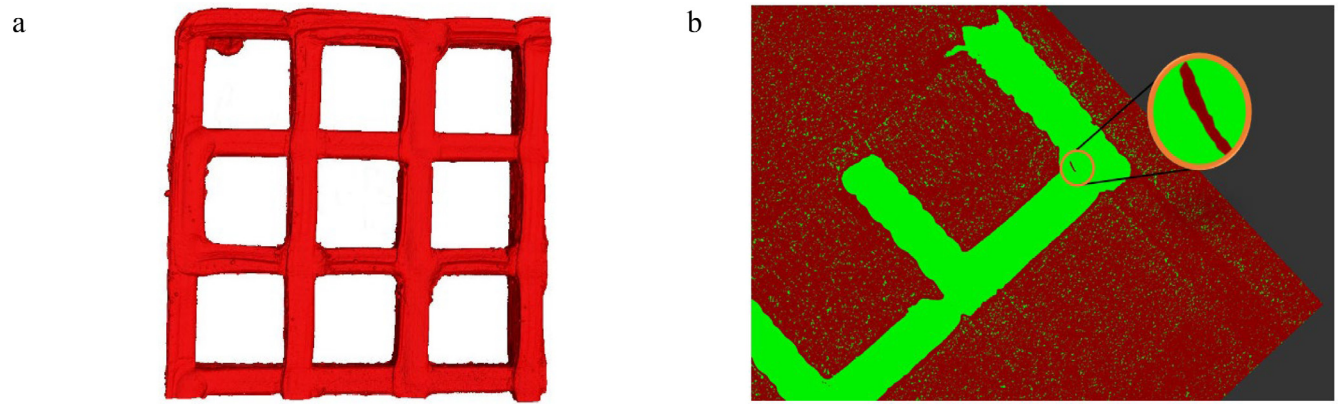

Fig. 5. X-ray micro-CT results: (a) Overall X-ray micro-CT image of specimen ID 5 and (b) Cross-section of specimen ID 5.

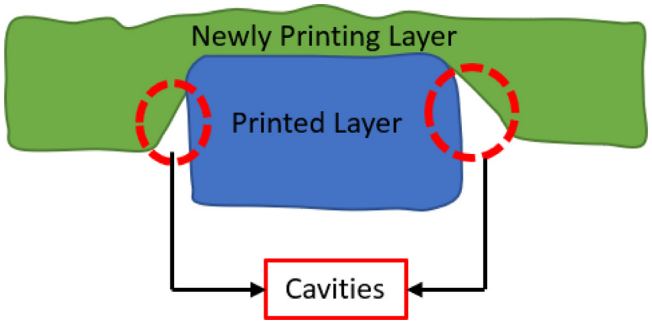

Fig. 6. Representation of cavity problem.

- On the other hand, extrusion speed was evaluated as one of the most prominent manufacturing parameters that change the microscale geometry of printed specimens. Observations showed that geometric instabilities such as distortion of the vertical and horizontal lines increased with increasing printing speed, as shown in Fig. 7.
- In addition to geometric instabilities, increasing printing speed also increased manufacturing defects, as shown in Fig. 7. Optical microscopy results clearly demonstrated that bulges occur around the vertical and horizontal lines with increasing printing speed.
- Over extrusion was observed for all the printed specimens shown in Figs. 7 and 8 for the cross-over points of vertical and horizontal lines. Moreover, the extrusion width of lines on these points varied significantly due to over-extrusion.
- Horizontal and vertical lines were offset in Z by half the layer height to overcome the over/under extrusion problem. The results showed that quality improved greatly. Also, differences in extrusion width between vertical and horizontal lines were reduced. The results support simulation results reported in the literature [13] and preliminary tensile-testing results indicate the potential for over twofold improvements in strength by offsetting crossing filament in Z by half the layer height.

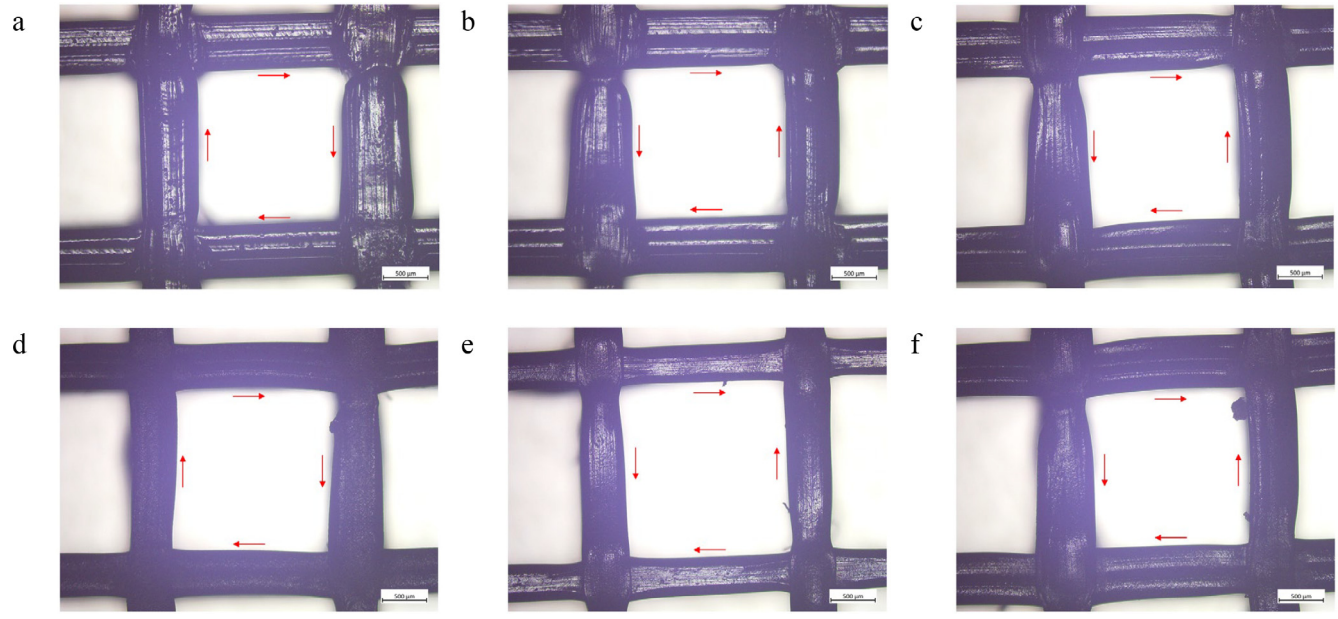

Fig. 7. Optical microscopy results for printing speed: (a) Printing speed 250, (b) Printing speed 500, (c) Printing speed 1000, (d) Printing speed 2000, (e) Printing speed 3000, and (f) Printing speed 4000.

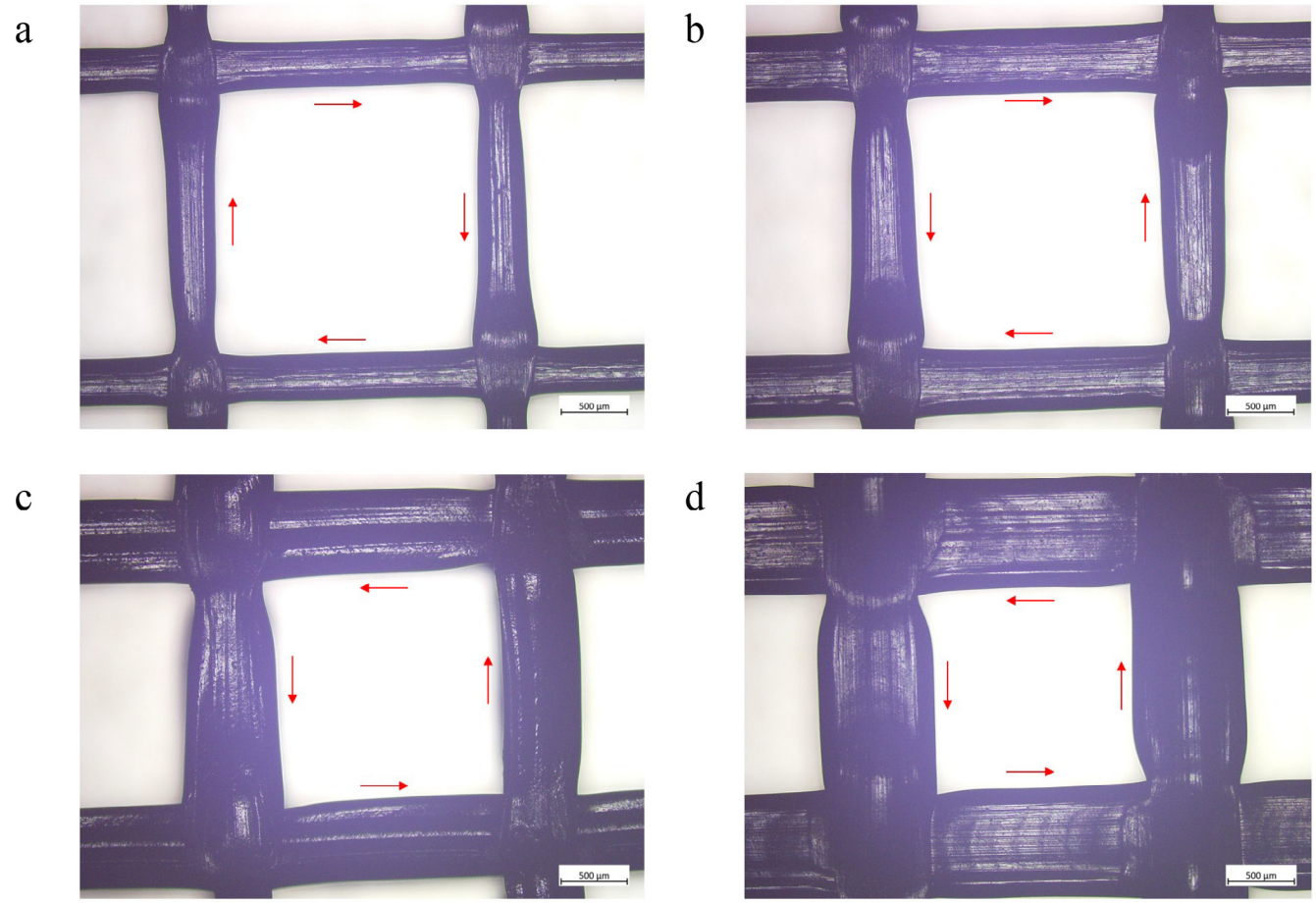

Fig. 8. Optical microscopy results for extrusion width: (a) Extrusion width 0.3 mm, (b) Extrusion width 0.4 mm, (c) Extrusion width 0.5 mm, and (d) Extrusion width 0.7 mm.

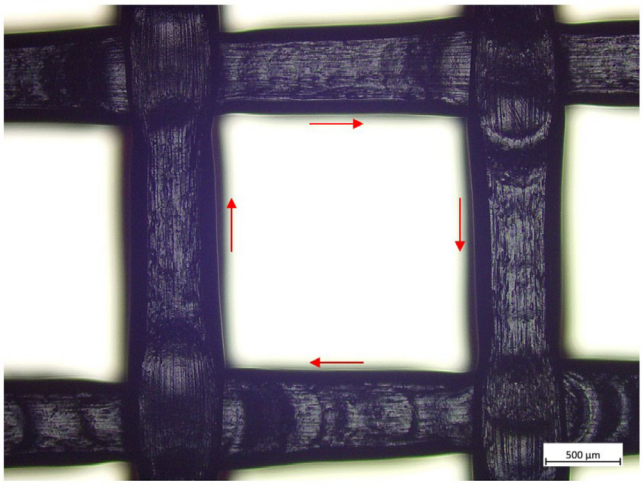

Fig. 9. Optical microscopy of specimen manufacturing with 0.1 mm distance between horizontal and vertical lines.

CRediT authorship contribution statement

Yagiz Kayali: Methodology, Visualization, Investigation, Formal analysis, Writing - original draft, Writing - review & editing. **Mingyang Ding:** Methodology. **Sheng Qi:** Conceptualization, Supervision, Writing - review & editing. **Richard Bibb:** Conceptualization, Supervision, Writing - review & editing. **Andrew Gleadall:** Conceptualization, Supervision, Methodology, Writing - review & editing.

Data availability

Data will be made available on request.

Declaration of Competing Interest

The authors declare that they have no known competing financial interests or personal relationships that could have appeared to influence the work reported in this paper.

Appendix A. Supplementary material

Supplementary material to this article can be found online at https://doi.org/10.1016/j.matpr.2022.08.487.

References

[1] S. Singh, S. Ramakrishna, Biomedical applications of additive manufacturing: Present and future, Curr. Opin. Biomed. Eng. 2 (2017) 105–115, https://doi.org/10.1016/J.COBME.2017.05.006.
[2] I. Zein, D.W. Hutmacher, K.C. Tan, S.H. Teoh, Fused deposition modeling of novel scaffold architectures for tissue engineering applications, Biomaterials 23 (2002) 1169–1185, https://doi.org/10.1016/S0142-9612(01)00232-0.
[3] T. Serra, J.A. Planell, M. Navarro, High-resolution PLA-based composite scaffolds via 3-D printing technology, Acta Biomater. 9 (2013) 5521–5530, https://doi.org/10.1016/J.ACTBIO.2012.10.041.
[4] J. Dirrenberger, S. Forest, D. Jeulin, Towards gigantic RVE sizes for 3D stochastic fibrous networks, Int. J. Solids Struct. 51 (2014) 359–376, https://doi.org/10.1016/j.ijsolstr.2013.10.011.

[5] S. Aslanzadeh, H. Saghlatoon, M.M. Honari, R. Mirzavand, C. Montemagno, P. Mousavi, Investigation on electrical and mechanical properties of 3D printed nylon 6 for RF/microwave electronics applications, Addit. Manuf. 21 (2018) 69–75, https://doi.org/10.1016/J.ADDMA.2018.02.016.

[6] K.C. Wong, S.M. Kumta, N.V.L. Gee, J. Demol, One-step reconstruction with a 3D-printed, biomechanically evaluated custom implant after complex pelvic tumor resection, Https://Mc.Manuscriptcentral.Com/Tcas. 20 (2015) 14–23, https://doi.org/10.3109/10929088.2015.1076039.

[7] X. Chen, L. Xu, Y. Wang, Y. Hao, L. Wang, Image-guided installation of 3D-printed patient-specific implant and its application in pelvic tumor resection and reconstruction surgery, Comput. Methods Programs Biomed. 125 (2016) 66–78, https://doi.org/10.1016/J.CMPB.2015.10.020.

[8] A. Duckworth, A. Gleadall, R. Bibb, Novel 3D printed custom kinesiology tape for variable usage scenarios, Trans. Addit. Manuf. Meets Med. 3 (2021) 540, https://doi.org/10.18416/AMMM.2021.2109540.

[9] J.M. Nasereddin, N. Wellner, M. Alhijjaj, P. Belton, S. Qi, Development of a Simple Mechanical Screening Method for Predicting the Feedability of a Pharmaceutical FDM 3D Printing Filament, Pharm. Res. 35 (2018), https://doi.org/10.1007/S11095-018-2432-3.

[10] M. Alhijjaj, J. Nasereddin, P. Belton, S. Qi, Impact of Processing Parameters on the Quality of Pharmaceutical Solid Dosage Forms Produced by Fused Deposition Modeling (FDM), Pharmaceutics 11 (12) (2019) 633.

[11] A. Gleadall, FullControl GCode Designer: Open-source software for unconstrained design in additive manufacturing, Addit. Manuf. 46 (2021) 102109, https://doi.org/10.1016/j.addma.2021.102109.

[12] FullControl GCODE Designer, (n.d.). http://fullcontrolgcode.com/ (accessed 28 March 2022).

[13] A. Gleadall, I. Ashcroft, J. Segal, VOLCO: A predictive model for 3D printed microarchitecture, Addit. Manuf. 21 (2018) 605–618, https://doi.org/10.1016/J.ADDMA.2018.04.004.